Nonlinear Dyn (2019) 97:2159–2174
https://doi.org/10.1007/s11071-019-05113-3

ORIGINAL PAPER

Chaotic system with bondorbital attractors

Xin Zhang · Chunhua Wang · Wei Yao · Hairong Lin

Received: 19 March 2019 / Accepted: 29 June 2019 / Published online: 10 July 2019

Abstract Two kinds of chaotic attractors with nontrivial topologies are found in a 4D autonomous continuous dynamical system. Since the equilibria of the system are located on both sides of the basic structures of these attractors, and the basic structures of these attractors are bond orbits, we call them bondorbital attractors. They have fractional dimensions and their Kaplan–Yorke dimensions are greater than 3. The generation mechanisms of the two types of attractors are explored and analyzed based on the Shilnikov's theorems. The type I attractors generated by system with parameter P_1 possess coexistence features, and the type II attractors generated by system with parameter P_2 have the ability to realize consecutive bond orbits. Furthermore, the type I attractors have continuous attracting basins with diagonal distribution and can be caught by means of a method of shorting capacitors in hardware experiments, whereas the type II attractors possess discrete basins of attraction and are difficult to be captured in hardware experiments. The difference between the two types of bondorbital attractors and traditional self-excited attractors in generation method is analyzed, and we also verify that they are not hidden attractors. Based on the step function sequence $f(x, M, N)$, the type II attractors with at most $(N + M + 1)$-fold structures can be generated in the system with parameter P_2. Two sets of symmetric specific initial conditions are used to verify that the system with parameter P_2 can generate bondorbital attractors with fourfold and fivefold basic structures based on $f(x, 2, 2)$. Some characteristics of the two classes of bondorbital attractors are listed in tabular form.

Keywords Bondorbital attractors · Bond orbits · Attracting basins · Multi-fold structures · Self-excited attractors · Hidden attractors

X. Zhang · C. Wang (✉) · W. Yao · H. Lin
College of Computer Science and Electronic Engineering, Hunan University, Changsha 410082, People's Republic of China
e-mail: wch1227164@hnu.edu.cn

X. Zhang
e-mail: zhangxin2302@126.com

W. Yao
e-mail: yaowei520026@sina.com

H. Lin
e-mail: haironglin@hnu.edu.cn

1 Introduction

Chaotic attractor, also known as strange attractor [1], is an abstract mathematical concept corresponding to the physical process of chaotic motion. The study for chaotic attractors helps us to understand the regularity of motion patterns in chaotic systems. Chaotic attractors have complex stretch and fold structures, which are the products of the overall stability and local instability of chaotic systems. From the topological structures they exhibit in phase space, the chaotic attractors associated with unstable equilibrium points can be categorized as familiar topological type (generally, including scroll

type, wing type, and torus type) and special topological type. The familiar type of chaotic attractors here refers to the chaotic attractors that have broad cognitive bases and were named for their topological structures in phase space. These two types of attractors are reviewed as follows.

(1) The type of attractors with familiar topologies

Chua's circuit built a bridge between nonlinear circuits and chaos for the first time, and the Chua attractor generated from it is a typical double-scroll chaotic attractor [2]. Suykens reported without precedent the use of quasi-linear approach to generate multi-scroll chaotic attractors based on the Chua system in [3]. In the jerk circuit, single-scroll and double-scroll chaotic attractors can be generated [4]. Yu proposed a nonlinear modulating function approach for generating multi-scroll chaotic attractors based on a general jerk circuit [5]. In addition, based on nonautonomous methods, multi-scroll and multi-double-scroll chaotic attractors can be generated in [6,7]. A kind of multi-scroll chaotic attractors with multi-attractor period and the corresponding chaotic integrated circuit (IC) based on current mode device were given in [8].

The generalize Lorenz system family is capable of generating two-wing chaotic attractors with very similar topologies [9–11]. The four-wing chaotic attractor was first generated based on the segmented Lorenz system and reported by Elwakil et al. [12,13]. Based on the generalized Lorenz system family, many ring-shaped, nested, and grid-shaped multi-wing chaotic attractors were generated from numerical simulations and hardware experiments in [14–19]. Moreover, a kind of multi-double-wing chaotic attractor was generated via a nonautonomous method in [20].

A double-folded torus chaotic attractor and its electronic circuit implementation were introduced in [21]. By expanding the double-folded torus chaotic attractor, a class of multi-folded torus chaotic attractors was obtained in [22]. In [23], the hardware circuit and experimental results of the single-torus and double-torus chaotic attractors were given. A class of grid-shaped multi-torus chaotic attractors, including numerical simulations and circuit experiments, was implemented in [24].

(2) The type of attractors with special topologies

A chaotic attractor with the projection on the $x - y$ plane similar to the shape of "trillium" was introduced in [25]. The literature [26] reported a number of multi-scroll, multi-folded torus chaotic attractors and some chaotic attractors with special topologies such as "multiple merged basins of attraction," "trillium," and "four-leaf clover." Simultaneously, a class of hyperchaotic attractors whose basic structures are "cluster-like" was also introduced in [26]. The literature [27] introduced a kind of strange attractors with toroidal topologies (i.e., van der Pol attractor). A chaotic attractor with 3D sphere shape was reported in [28]. A chaotic attractor whose topology resembles a cord between two leaves was called cord attractor [29]. By performing coordinate transformations on the Sprott E system, [30] found chaotic attractors with "petal" topologies. A double-deck butterfly chaotic attractor whose topology is similar but different from the nested and grid-shaped four-wing chaotic attractors was reported in [31]. By performing fractal process on Qi system [32], [33] reported a class of 3D spherical multi-wing chaotic attractors. Based on the 2D local vector field around equilibria, [34] reported several chaotic attractors with "nested" topologies.

Among the above-mentioned chaotic attractors with familiar and special topologies, the unstable equilibria (saddle-foci with index 1 or 2) of them are located within their respective basic structures. In this paper, we find two kinds of chaotic attractors with nontrivial topologies, whose unstable equilibria lie on both sides of the basic structures of these attractors. Theoretical analysis shows that the two kinds of attractors have very fast spiral motions and slow linear motions near their equilibrium points, resulting in the formation of fully bond orbits. Since the basic structures of the attractors are fully bond orbits between two adjacent homogeneous saddle-focus equilibria with index 1, we name the two kinds of chaotic attractors as bondorbital attractors. The body widths of the type I attractors in the x direction are smaller than the distance between the adjacent two equilibria and therefore have coexistence characteristics on the basis of a step function sequence. Due to their larger maximum LEs and Kaplan–Yorke dimensions, the type II attractors possess the ability to realize continuous bond orbits between homogeneous equilibria. Interestingly, the two kinds of bondorbital attractors have Kaplan–Yorke dimensions greater than 3, one of which has uninterrupted attracting basins with zonal distribution and the other of which possesses discrete attracting basins. We also prove that the bondorbital attractors found in this paper are different from existing self-excited attractors and hidden attractors.

As far as I know, such chaotic attractors have not been reported in available researches.

The rest of this paper is organized as follows. The numerical model of the proposed chaotic system, the illustration of topologies for bondorbital attractors, the dynamical analysis for chaotic system with bondorbital attractors, and the study of generation mechanism for bondorbital attractors are all included in Sect. 2. In Sect. 3, the hardware validation for one of type I attractors and some researches of characteristics for the attracting basins of the two types of bondorbital attractors are given. Section 4 demonstrates the type II attractors have discrete basins of attraction and possess structural repeatability. Section 5 summarizes the main characteristics of the two types of bondorbital attractors. Finally, some conclusions of our paper are given in Sect. 6.

2 Chaotic system with bondorbital attractors

2.1 Two types of bondorbital attractors

The state variable equation of four-dimensional dynamical system is given by

$$\begin{cases} \dot{x} = ay, \\ \dot{y} = by + cz, \\ \dot{z} = d\left[-x - y - z + f(x, M, N)\right], \\ \dot{w} = eyzw - x + f(x, M, N), \end{cases} \tag{1}$$

where a, b, c, d, and e are system parameters, x, y, z, and w are four state variables, and $f(x, M, N)$ is a nonlinear function, here step function sequence (SFS), and its expression is

$$f(x, M, N) = (N - M)\, A_2 + A_2 \left[\begin{array}{l} \operatorname{sgn}(x) + \sum_{j=1}^{M} \operatorname{sgn}(x + 2jA_1) \\ + \sum_{i=1}^{N} \operatorname{sgn}(x - 2iA_1) \end{array} \right], \tag{2}$$

where M and N are nonnegative integers and the width and height of each step are $2A_1$ and $2A_2$, respectively. In this paper, we make A_1 and A_2 equal to 1 in all numerical simulations. When $M = N = 1$, the numerical curve of the SFS $f(x, 1, 1)$ is shown in Fig. 1.

Based on $f(x, 1, 1)$, and if system parameter $P_1 = (a, b, c, d, e) = (-1, 0.2, 1, 1.1, 0.001)$ is chosen in system (1), the 2D views of two attractors are shown

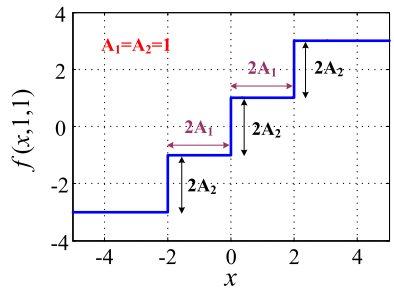

Fig. 1 Numerical curve of the SFS $f(x, M, N)$, where $M = N = 1$ and $A_1 = A_2 = 1$

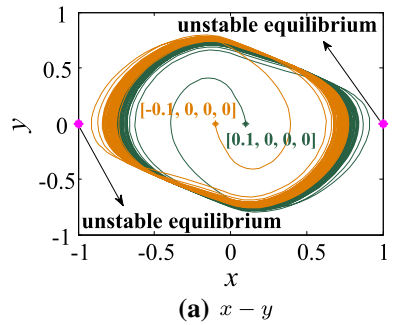

(a) $x - y$

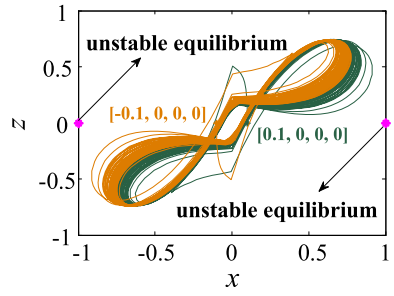

(b) $x - z$

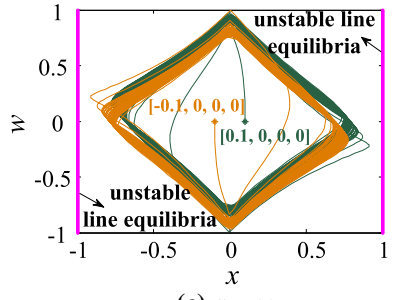

(c) $x - w$

Fig. 2 Superimposed 2D views of two symmetric bondorbital attractors in **a** $x - y$, **b** $x - z$, and **c** $x - w$ plane under two symmetric initial conditions [0.1, 0, 0, 0] and [− 0.1, 0, 0, 0] when P_1 is selected

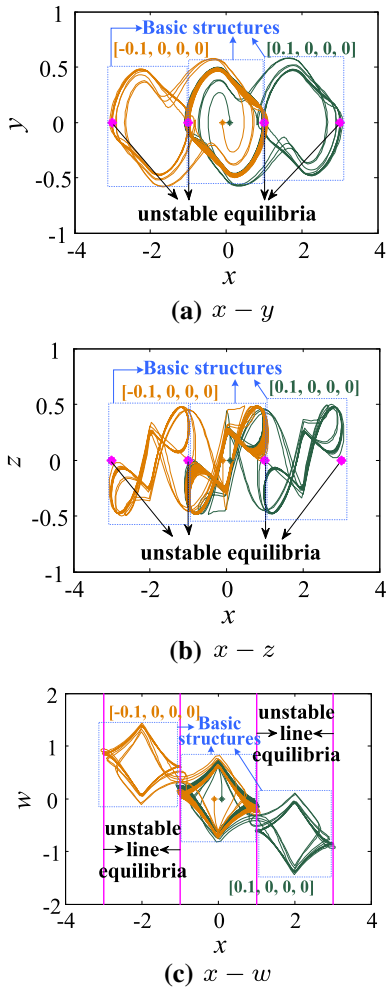

Fig. 3 Superimposed 2D views of two symmetric bondorbital attractors in **a** $x-y$, **b** $x-z$, and **c** $x-w$ plane under two symmetric initial conditions [0.1, 0, 0, 0] and $[-0.1, 0, 0, 0]$ when P_2 is set

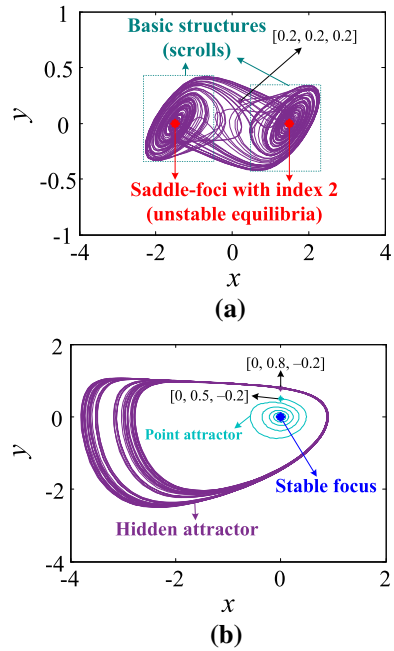

Fig. 4 **a** 2D $x-y$ plane view of Chua double-scroll attractor under initial condition [0.2, 0.2, 0.2]; **b** 2D $x-y$ plane views of hidden and point attractors in SE_9 system under initial conditions [0, 0.8, -0.2] and [0, 0.5, -0.2], respectively

in Fig. 2. In Fig. 2, two symmetric initial conditions $[-0.1, 0, 0, 0]$ and [0.1, 0, 0, 0] are used to generate the two symmetric (with regard to the origin) attractors. From Fig. 2, the unstable equilibria are located on both sides of the attractors. If system parameter $P_2 = (-2.08, 0.2, 1, 1.1, 0.001)$ is set, the 2D views of two symmetric attractors with initial conditions $[-0.1, 0, 0, 0]$ and [0.1, 0, 0, 0] are shown in Fig. 3. In addition, it is interesting to note that the attractors shown in Fig. 3 are basically twice structural extension of the attractors in Fig. 2. We take the topologies of the attractors shown in Fig. 2 as the basic structures (marked by dashed boxes) of the attractors shown in Fig. 3. Obviously, the unstable equilibria are located on both sides of the basic structures of the attractors. In Figs. 2 and 3, we mark the unstable equilibrium points of the system by magenta points or lines within the simulated coordinate region.

According to available researches, chaotic attractors associated with unstable equilibria, such as traditional scroll, wing, and torus attractors, have basic structures generated around a single unstable equilibrium point [2–34]. As an example, we simulate the dimensionless Chua system in [35] for parameters $(\alpha, \beta, m_0, m_1) = (10, 15, -1/7, 2/7)$ under initial condition [0.2, 0.2, 0.2] and then obtain the 2D $x-y$ plane view of Chua double-scroll attractor shown in Fig. 4a. As can be clearly seen from Fig. 4a, the two saddle-focus equilibria with index 2 are located within the basic structures (scrolls) of the attractor, respectively. However, the unstable equilibria of the bondorbital attractors are located on both sides of their basic structures, as shown in Figs. 2 and 3.

An attractor is called a hidden attractor if its basin of attraction does not intersect with any open neighborhood of equilibria, or otherwise it is called a self-excited

Table 1 The distribution of x^E under different parameters of (2)

Nonlinear function	Number of equilibria	Parameters of (2)	Numeric values of x^E	Distribution rule
SFS $f(x, M, N)$	Infinite equilibrium points	$M = N = 0$	$-1, 1$	$-2\mathrm{M}-1, -2M+1, \ldots,$
		$M = N = 1$	$-3, -1, 1, 3$	$-1, 1, \ldots,$
	$(x^E, 0, 0, l)$	$M = 2, N = 3$	$-5, -3, -1, 1, 3, 5, 7$	$2N-1, 2N+1$

attractor [36–38]. According to the definition of hidden attractors, chaotic attractors in systems with no equilibrium [39,40] or only stable equilibriums [41] are deterministic hidden attractors, whereas chaotic attractors in systems with infinite equilibriums do not fully satisfy the definition of hidden attractors (whose basins of attraction may intersect with some equilibria) [42,43]. We simulate the SE_9 system with hidden attractors proposed in [41], as shown in Fig. 4b, where the equilibrium is marked by blue point. In Fig. 4b, initial condition $[0, 0.8, -0.2]$ leads to hidden attractor, whereas initial condition $[0, 0.5, -0.2]$ leads to point attractor. It should be noted that the attractors in Figs. 2 and 3 are related to system equilibria (the attracting basins of our discovered attractors intersect with system equilibria, see Fig. 12 and the corresponding illustrations in Sect. 3), which are different from hidden attractors (see Fig. 13, in which the attracting basin of the hidden attractor does not intersect with system equilibrium).

2.2 Equilibrium calculation and stability analysis

Let $\dot{x} = \dot{y} = \dot{z} = \dot{w} = 0$, the equilibrium points of system (1) can be derived by solving

$$\begin{cases} ay = 0, \\ by + cz = 0, \\ d\left[-x - y - z + f(x, M, N)\right] = 0, \\ eyzw - x + f(x, M, N) = 0. \end{cases} \tag{3}$$

From (3), it can be concluded that as long as all system parameters are nonzero, the corresponding solution is $E^Q = (x^E, 0, 0, l)$, in which we use a line l to indicate that the state variable w can take any constant value, and the value of x^E depends on the form and parameters of the nonlinear function $f(x, \mathrm{M}, \mathrm{N})$. The calculation result shows that the system has infinite equilibria.

We use (2) as an example to analyze the distribution of equilibrium points in x direction. For different parameters of (2), Table 1 shows several specific values and the overall distribution law of x^E.

The Jacobian matrix of system (1) combining (2) at the equilibrium point $E^Q = (x^E, 0, 0, l)$ can be expressed as

$$J\left(E^Q\right) = \left[\begin{array}{cccc} 0 & a & 0 & 0 \\ 0 & b & c & 0 \\ -d + df'(x, M, N) & -d & -d & 0 \\ -1 + f'(x, M, N) & ezw & eyw & eyz \end{array}\right]\Bigg|_{E^Q} = \begin{bmatrix} 0 & a & 0 & 0 \\ 0 & b & c & 0 \\ -d & -d & -d & 0 \\ -1 & 0 & 0 & 0 \end{bmatrix}. \tag{4}$$

An interesting phenomenon can be drawn from (4) that although the system has infinite equilibrium points, the Jacobian matrix at the equilibria of this system is independent of the positions of state variable w in these equilibrium points. This is different from many of the chaotic systems with infinite equilibria that have been reported [42,43].

Solving $\left|\lambda\mathbf{E} - J\left(E^Q\right)\right| = 0$, where $\mathbf{E}$ is an identity matrix, one can get that the characteristic roots of system (1) at E^Q satisfy

$$\lambda\left[\lambda^3 + (d-b)\lambda^2 + (c-b)d\lambda + acd\right] = 0, \tag{5}$$

where one of the solutions is zero, and the other three satisfy

$$\lambda^3 + (d-b)\lambda^2 + (c-b)d\lambda + acd = 0. \tag{6}$$

The algebraic solutions of (6) can be obtained as per the extract roots formula of the generalized unary cubic equation, but the result is too complicated to win effective information for analysis. Therefore, we utilize the relationship between roots and coefficients (Cardano's formula [44]) to analyze the stability of the system. For (6), one have

$$\begin{cases} \lambda_1 + \lambda_2 + \lambda_3 = b - d, \\ \lambda_1\lambda_2 + \lambda_2\lambda_3 + \lambda_1\lambda_3 = (c-b)d, \\ \lambda_1\lambda_2\lambda_3 = -acd. \end{cases} \tag{7}$$

Assume that all roots of (6) are in the left half plane of the complex plane (stable solution), and the following relationship can be obtained [38].

Table 2 The corresponding eigenvalues and stabilities when a takes several typical values ($b = 0.2, c = 1, d = 1.1, e = 0.001$)

Typical values of a	Eigenvalues	Stabilities
1	$-1.055, 0.077 \pm 1.018j, 0$	Saddle-foci with index 2 (unstable)
0.72	$-0.9, \pm 0.938j, 0$	Hopf bifurcation (nonhyperbolic equilibrium)
0.5	$-0.728, -0.086 \pm 0.865j, 0$	Stable focus
0	$0 - 0.450 \pm 0.823j, 0$	Critical stable
-1 (P_1)	$0.610, -0.755 \pm 1.110j, 0$	Saddle-foci with index 1 (unstable)
-2.08 (P_2)	$0.908, -0.904 \pm 1.305j, 0$	

$$\begin{cases} b - d < 0, \\ (c - b)d > 0, \\ -acd < 0. \end{cases} \tag{8}$$

If a is uncertain and other parameters are respectively $b = 0.2, c = 1, d = 1.1$, and $e = 0.001$, then $b - d = -0.9 < 0$, $(c - b)d = 0.88 > 0$, and $-acd = -1.1a$. This shows that system (6) is stable as long as $a > 0$. However, after substituting specific values for calculation, it is found that this method is not completely feasible. A more appropriate way to judge the stability of a system is the Routh–Hurwitz criterion [45]. To determine a, the Routh table of (6) is given by

$$\begin{array}{c|cc} \lambda^3 & 1 & 0.88 \\ \lambda^2 & 0.9 & 1.1a \\ \lambda^1 & \frac{0.792 - 1.1a}{0.9} & 0 \\ \lambda^0 & 1.1a & 0 \end{array}. \tag{9}$$

Therefore, if there is no sign change in the second column of (9), namely $0 < a < 0.72$, the system is stable. If $a < 0$, only one of the three roots of (6) has a positive real part. If $a > 0.72$, two of the three roots of (6) have positive real parts. We list the characteristic roots corresponding to (5) when a takes several typical values, as given in Table 2.

2.3 Lyapunov exponent spectrum with respect to parameter a

The Lyapunov exponent spectrum of system (1) with respect to a (with other system parameters $b = 0.2, c = 1, d = 1.1, e = 0.001$) is shown in Fig. 5. In the simulation of the Lyapunov exponents (LEs), the continuous differentiable arc-tangent function $a\tan(B(x)/(\pi/2))$ is used to approximate the discontinuous differentiable sign function $sgn(x)$, in

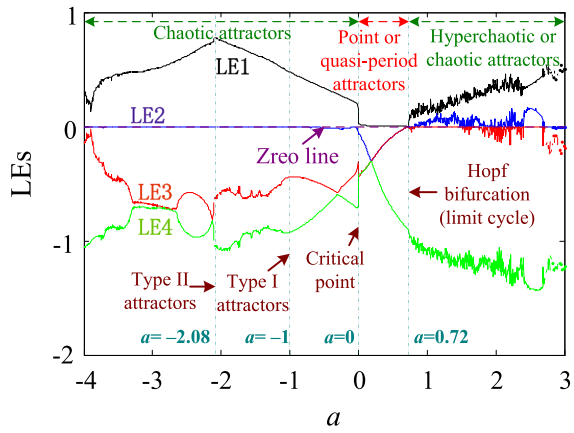

Fig. 5 Lyapunov exponent spectrum of system (1) for $a \in (-4, 3)$ under initial conditions $[\pm 0.1, 0, 0, 0]$

which we set $B = 1000$ to obtain good approximation. The famous Wolf algorithm is adopted in the simulation [46]. There are three main regions in Fig. 5:

Region 1 for $-4 < a < 0$, LE1 > 0, LE2 $= 0$, LE3 < 0, and LE4 < 0.

Region 2 for $0 < a < 0.72$, LE1 $= 0$, LE2 ≤ 0, LE3 ≤ 0, and LE4 < 0.

Region 3 for $0.72 < a < 3$, LE1 ≥ 0, LE2 ≥ 0, LE3 ≤ 0, and LE4 < 0.

Therefore, the motion trajectories of the system successively appear as chaotic attractors, point attractors, quasi-period attractors, limit cycles, hyperchaotic attractors, and so on, with the increase in a. Therefore, the two kinds of bondorbital attractors found in this paper are indeed chaotic according to the definition of chaos.

For convenience, we refer to the chaotic attractors in Figs. 2 and 3 as type I and II attractors, respectively. With the initial conditions $[\pm 0.1, 0, 0, 0]$, the type I attractors have LEs = $(0.466, 0, -0.430, -0.935)$

with Kaplan–Yorke dimensions $D_{\mathrm{KY}} = 3.038$ and the type II attractors possess LEs = $(0.774, 0, -605, -1.068)$ with $D_{\mathrm{KY}} = 3.158$. ($D_{\mathrm{KY}} = j + \frac{1}{|\mathrm{LE}_{j+1}|}\sum_{i=1}^{j}\mathrm{LE}_i$, where j is the largest integer which satisfies $\sum_{i=1}^{j}\mathrm{LE}_i \geq 0$ and $\sum_{i=1}^{j+1}\mathrm{LE}_i < 0$, and LE_i for $i = 1, 2, \ldots, 4$ are Lyapunov exponents that are sorted from largest to smallest [47].) The four-dimensional chaotic attractors are not hyperchaotic, whereas they have Kaplan–Yorke dimensions greater than 3, which indicates that the bondorbital attractors possess unusual dynamical behaviors. It is worth noting that the system has a largest positive LE1 when $a = -2.08$, which means that the local instability of the system is the largest.

2.4 Generation mechanisms of the two classes of bondorbital chaotic attractors

Further exploration of the generation mechanisms about the two kinds of bondorbital attractors is needed. When the system with parameter P_1 is tested by a loop test algorithm (iteration of initial conditions), attractors with multi-fold structures (like in Fig. 3) cannot be generated, no matter how many tests are performed. In order to understand the generation mechanisms of the bondorbital attractors, we try to start the analysis from the Shilnikovs theorems. The following are two statements about the Shilnikovs theorems [48] (applicable to the saddle-foci with index 1 or 2):

Theorem 1 (Shilnikov Theorem 2.1) [49] *When a third-order autonomous dynamical system satisfies the following two conditions simultaneously, there exist chaos in the sense of Smale horseshoe: (i) The linearized coefficient matrix of an orbit at its equilibrium point O has a pair of complex conjugate eigenvalues (CCEs) $\sigma \pm j\omega$ and a real eigenvalue γ and satisfies $|\sigma/\gamma| < 1$; (ii) there exists a homoclinic orbit that starts from the equilibrium point O and finally returns to this equilibrium point.*

Theorem 2 (Shilnikov Theorem 2.2) [49] *When a third-order autonomous dynamical system satisfies the following two conditions simultaneously, there exist chaos in the sense of Smale horseshoe: (i) The linearized coefficient matrixes of two different orbits at their corresponding equilibrium points $O_i (i = 1, 2)$ have respective a pair of CCEs $\sigma_i \pm j\omega_i (i = 1, 2)$ and a real eigenvalue $\gamma_i (i = 1, 2)$, and satisfy $\gamma_1\gamma_2 > 0, \sigma_1\sigma_2 > 0$, and $|\sigma_i/\gamma_i| < 1 (i = 1, 2)$; (ii) there exists a heteroclinic orbit connecting two equilibrium points O_1 and O_2.*

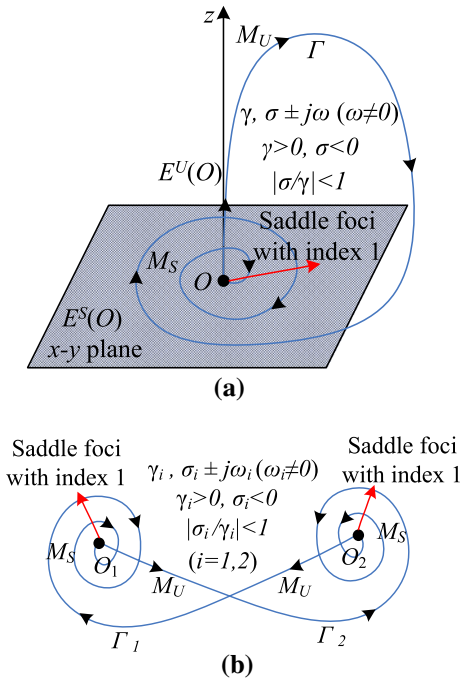

Fig. 6 Saddle-foci with index 1 and its **a** homoclinic and **b** heteroclinic orbits

The inequalities $|\sigma/\gamma| < 1$ and $|\sigma_i/\gamma_i| < 1 (i = 1, 2)$ in the two theorems are both called Shilnikov inequalities, which correspond to the judgment of the homoclinic and heteroclinic orbits. According to Table 2, the equilibria of the system with parameter P_1 and P_2 are saddle-foci with index 1. Therefore, for the sake of simplicity, only graphical descriptions for the homoclinic and heteroclinic orbits of the saddle-foci with index 1 are given, as shown in Fig. 6.

We use λ_i $(i = 1, 2, 3)$ to indicate the eigenvalues of systems at their equilibrium points, where $\lambda_1 = \gamma, \lambda_{2,3} = \sigma \pm j\omega$. In Fig. 6a, b, associated with the saddle-foci with index 1 are a 2D eigenplane $E^S(O)$ corresponding to the CCEs $\sigma \pm j\omega$ with negative real part and a 1D eigenline $E^U(O)$ corresponding to the positive real eigenvalue γ. Therefore, this type of equilibrium points presents a stable manifold $M_S = \mathrm{span}\{V_{\lambda 2}, V_{\lambda 3}\}$ and an unstable manifold $M_U = \mathrm{span}\{V_{\lambda 1}\}$, in which $V_{\lambda i}$ corresponds to the eigenvector of the linearized coefficient matrixes of systems regarding the eigenvalue λ_i.

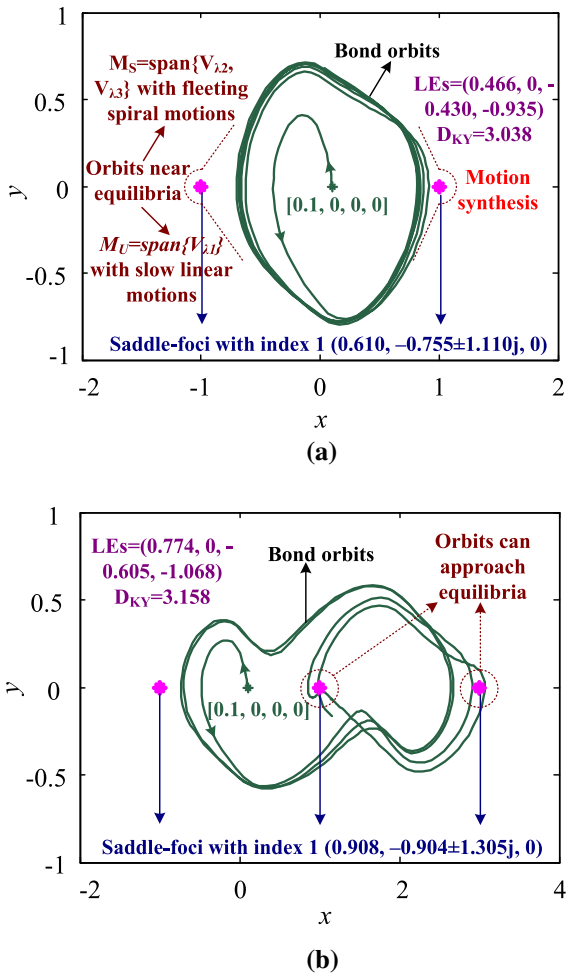

Fig. 7 2D $x-y$ plane views of motion diagrams of the **a** type I and **b** type II attractors within a very short simulation time under initial condition [0.1, 0, 0, 0]

It should be noted that in order to make the statements of these two theorems concise and easy to understand, the two theorems are aimed at 3D autonomous dynamical system (the minimum requirements of dimensions on generating chaos in autonomous systems). However, these results have proven to be equally applicable to higher-dimensional dynamical systems [50]. Furthermore, our proposed 4D system has a zero eigenvalue at all equilibria, which means that the overall trajectory would not be affected from the incidental eigenline.

For a better presentation, Fig. 7 shows the 2D $x-y$ plane views of the type I and type II attractors within a very short simulation time under initial condition [0.1, 0, 0, 0]. From Table 2, the CCEs of the system

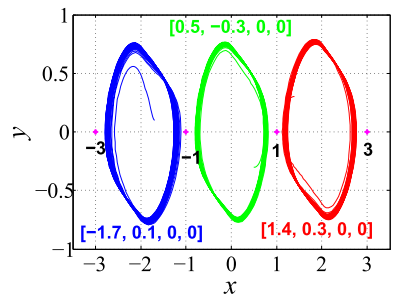

Fig. 8 Coexisting type I attractors in $x-y$ plane, where $[-1.7, 0.1, 0, 0]$ leads to blue orbits, $[0.5, -0.3, 0, 0]$ leads to green orbits, and [1.4, 0.3, 0, 0] leads to red orbits. (Color figure online)

at their equilibria (under parameters P_1 and P_2) possess relatively large absolute values of real parts (can be denoted by $|Re\{\lambda_{2,3}\}|$) and $|\sigma/\gamma|$, which are bigger than the counterparts in most of available chaotic systems [51,52]. Moreover, based on prior knowledge, the motion trails in 2D eigenplane near the equilibria are governed by the real parts of the CCEs at these equilibrium points. Therefore, the stable manifolds $M_S = \text{span}\{V_{\lambda 2}, V_{\lambda 3}\}$ of the type I and type II attractors near the equilibria have fast spiral motions, or even fleeting motions in their eigenplanes. Finally, 2D stable manifolds $M_S = \text{span}\{V_{\lambda 2}, V_{\lambda 3}\}$ with very fast spiral motions and 1D unstable manifolds $M_U = \text{span}\{V_{\lambda 1}\}$ with slow linear motions synthesize the attractors with nontrivial shapes shown in Figs. 2 and 3.

The four eigenvalues of the system with parameter P_1 at all equilibrium points are $\lambda_1 = \gamma = 0.610$, $\lambda_{2,3} = \sigma \pm j\omega = -0.755 \pm 1.110j$, and $\lambda_4 = 0$. Although the system has motion trajectories with plausible heteroclinic loop in this case, whereas $|\sigma/\gamma| > 1$ does not satisfy the Shilnikov inequality, the type I attractors are not the chaos in the sense of Smale horseshoe. We again analyze and compare Fig. 7a, b and find that the plausible heteroclinic loops of the bondorbital attractors in Fig. 7a cannot reach the adjacent two equilibria completely (-1 and $+1$ in x-direction). Therefore, it is difficult to copy or expand the structures of the type I attractors by changing the initial values. On the contrary, we naturally think that the system with parameter P_1 can generate coexisting attractors under different initial conditions, as shown in Fig. 8.

The four eigenvalues of the system with parameter P_2 at all equilibria are $\lambda_1 = \gamma = 0.908$, $\lambda_{2,3} = \sigma \pm j\omega = -0.904 \pm 1.305j$, and $\lambda_4 = 0$. Apparently, due to $|\sigma/\gamma| < 1$ and the existed heteroclinic loops

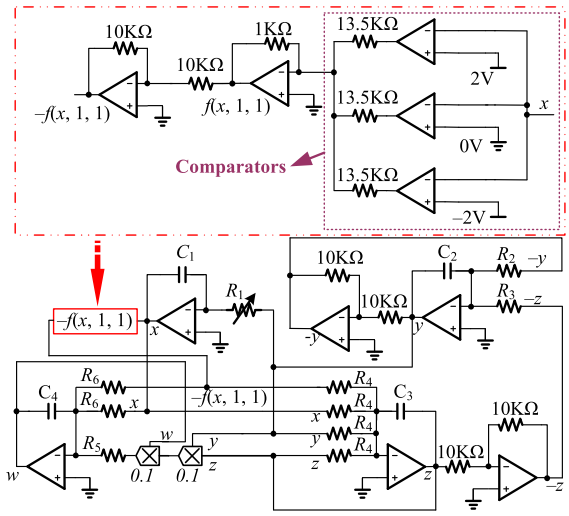

Fig. 9 Circuit schematic diagram

(bond orbits), the system has the chaotic behaviors explained from Smale horseshoe theory. From Fig. 5, the maximum LE and Kaplan–Yorke dimension of the system with parameter P_2 are obviously larger than those of the system with parameter P_1. Due to its larger local instability and higher fractional dimensions, it can be inferred that the motion trajectories of the system with parameter P_2 have the ability to realize continuous bond orbits between homogeneous equilibrium points. Since we used a four-step SFS $f(x, 1, 1)$ in previous simulations, we suspect whether different initial conditions will generate bondorbital attractors with different shapes in the system with parameter P_2. Inspired by the subsequent hardware experiments, we find that this is indeed the case and get more conclusions.

3 Validate attractors by constructing hardware circuits

It is necessary to perform physical verification for the attractors of the foregoing simulations, and the hardware experiment reproduces the attractors is a credible method. Op-amp TL082CP, multiplier AD633JN, resistor, and monolithic ceramic capacitor are combined on breadboard for capturing the attractors. The schematic diagram of the designed circuit is shown in Fig. 9, where x, y, z, and w represent the voltages across capacitors C_1, C_2, C_3, and C_4, respectively. The circuit equations according to the circuit schematic diagram are given by

$$\begin{cases} C_1 \cdot \mathrm{d}x/\mathrm{d}t = -y/R_1, \\ C_2 \cdot \mathrm{d}y/\mathrm{d}t = y/R_2 + z/R_3, \\ C_3 \cdot \mathrm{d}z/\mathrm{d}t = [-x - y - z + f\,(x, 1, 1)]/R_4, \\ C_4 \cdot \mathrm{d}w/\mathrm{d}t = 0.01 \cdot yzw/R_5 - [x - f\,(x, 1, 1)]/R_6. \end{cases} \tag{10}$$

If we introduce a time factor $1/R_0C_0$ in system (1), its form will be transformed into

$$\begin{cases} C_0 \cdot \mathrm{d}x/\mathrm{d}t = ay/R_0, \\ C_0 \cdot \mathrm{d}y/\mathrm{d}t = by/R_0 + cz/R_0, \\ C_0 \cdot \mathrm{d}z/\mathrm{d}t = d\,[-x - y - z + f\,(x, M, N)]/R_0, \\ C_0 \cdot \mathrm{d}w/\mathrm{d}t = eyzw/R_0 - [x - f\,(x, M, N)]/R_0. \end{cases} \tag{11}$$

For system with parameter P_1, we set $R_0 = 20\,\mathrm{K\Omega}$ and $C_1 = C_2 = C_3 = C_4 = C_0 = 10\,\mathrm{nF}$; the resistance values of the other resistors can be obtained by comparing (10) and (11)

$$\begin{cases} -1/R_1 = a/R_0 \rightarrow R_1 = -R_0/a = 20\,\mathrm{K\Omega}, \\ 1/R_2 = b/R_0 \rightarrow R_2 = R_0/b = 100\,\mathrm{K\Omega}, \\ 1/R_3 = c/R_0 \rightarrow R_3 = R_0/c = 20\,\mathrm{K\Omega}, \\ 1/R_4 = d/R_0 \rightarrow R_4 = R_0/d = 18.18\,\mathrm{K\Omega}, \\ 0.01/R_5 = e/R_0 \rightarrow R_5 = 0.01 \cdot R_0/e = 200\,\mathrm{K\Omega}, \\ 1/R_6 = 1/R_0 \rightarrow R_6 = R_0 = 20\,\mathrm{K\Omega}. \end{cases} \tag{12}$$

Based on the circuit schematic diagram and the calculated component values in (12), we perform the wiring of the discrete components on breadboard and first observe the experimental result of $f(x, 1, 1)$, as shown in Fig. 10. In Fig. 10, except for the two analog multipliers labeled with AD633JN, all other chips are TL082CP. The number of steps of the SFS circuit within the blue dashed box can be adjusted by increasing or decreasing the number of comparators (also composed of op-amps, like in Fig. 9). In this experiment, a clear four-step waveform can be observed from the oscilloscope in Fig. 10.

In general, the visual presentation of type I attractors can be implemented with hardware experiments. At the beginning, the expected attractor image does not appear. Therefore, we use the instantaneous shorting of the two pins of C_1 to approximate the initial values listed in Fig. 2 (means draw near the attracting basins of the type I attractors), thus obtaining the one of type I attractors shown in Fig. 11.

We change the value of R_1 to 9.62 KΩ (i.e., system with parameter P_2) to exhibit the type II attractors by hardware experiment, but find that the same method of shorting capacitors does not work. A seemingly correct attractor image appears only when one or several of the capacitors are shorted and then released, but it cannot be stabilized in the motion state of the type II attractors. Therefore, it is necessary to compare the basins of

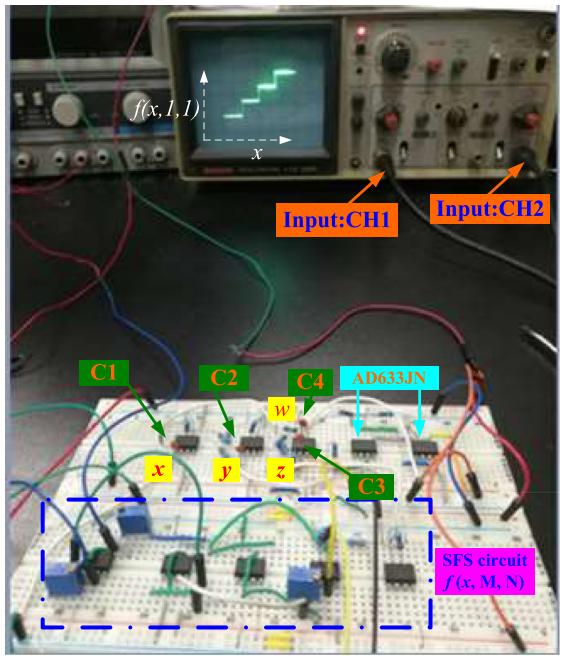

Fig. 10 Wire diagram of the hardware circuit on breadboard and experimental result of $f(x, 1, 1)$ on site (where CH1 and CH2 are $1V/\text{div}$)

attraction of the type I and type II attractors to see why we cannot use hardware to achieve the type II attractors in steady state, as shown in Fig. 12. In Fig. 12a, b, the initial values $x(0)$ and $y(0)$ have an iteration point of 401, so the step sizes are 0.05.

It can be seen from Fig. 12a that the three colored attracting basins of the type I attractors are diagonally distributed, which are larger near the origin and gradually narrower toward the two diagonal positions. So we can use a method of shorting capacitors to make the initial state approaching the basins of attraction to obtain the type I attractors in hardware experiments. However, some sporadic discrete points with various colors (basins of attraction) are scattered in Fig. 12b, which occupy a smaller areas and are included in the white dashed box. A portion of the basins of unbounded motions are located between these discrete attracting basins. When these discrete basins of attraction are validated by choosing several specific initial conditions, they are found to be incomplete basins of attraction. (It is difficult to simulate the completed basins of attraction, as will be explained in the next section.) The discrete basins of attraction are sufficient to show that the initial conditions are too harsh in this case. In consequence, it is difficult to implement the type II attractors based on hardware experiments.

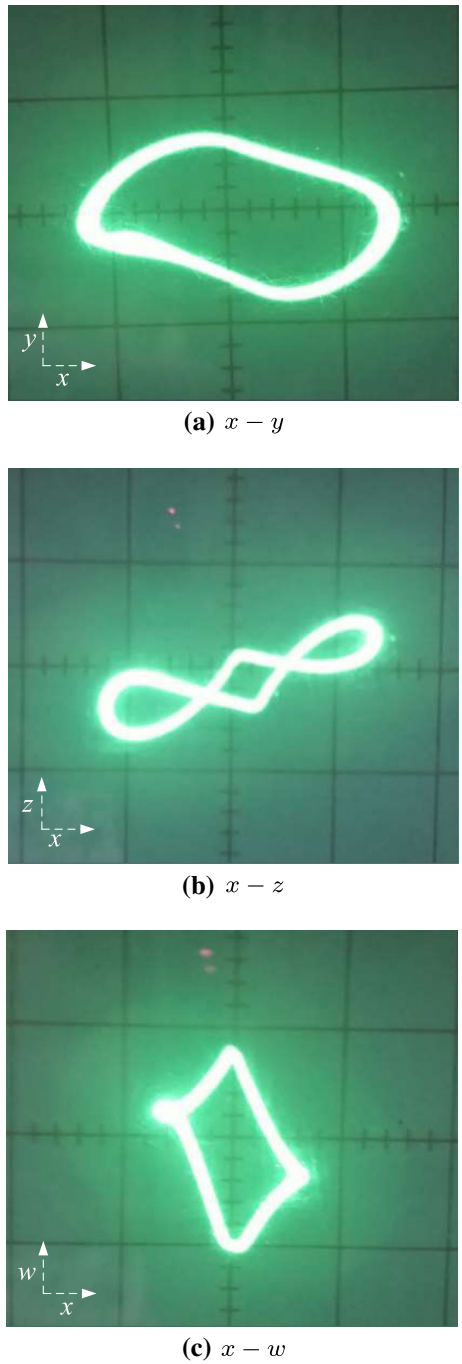

(a) $x - y$

(b) $x - z$

(c) $x - w$

Fig. 11 One of type I attractors in **a** $x - y$, **b** $x - z$, and **c** $x - w$ plane (where x, y, and z are $1V/\text{div}$)

For comparison, we simulate the attracting basins of the SE_9 system with hidden attractors proposed in [41],

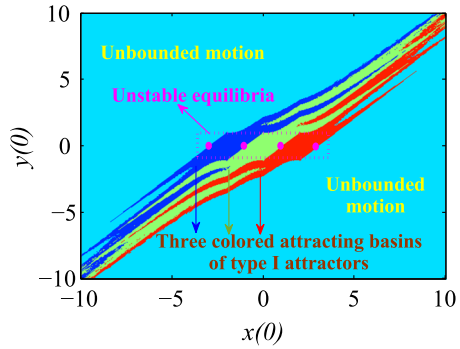

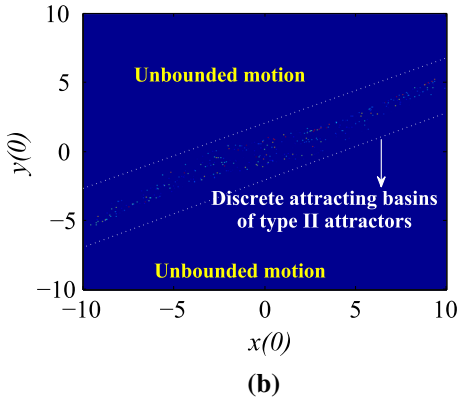

Fig. 12 Cross sections of attracting basins at $z(0) = w(0) = 0$ in $x(0) - y(0)$ plane for system with parameters **a** P_1 and **b** P_2, where $x(0), y(0) \in (-10, 10)$

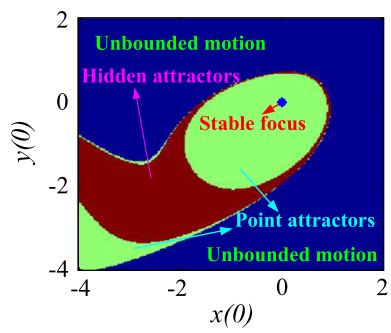

Fig. 13 Cross section of the basins of attraction of the SE_9 system in [41] at $z(0) = 0$ in $x(0) - y(0)$ plane, where $x(0), y(0) \in (-4, 2)$

as shown in Fig. 13, in which the attracting basins of point attractors, hidden attractors, and unbounded motion are marked. Obviously, the basin of attraction of the hidden attractor does not intersect with the stable focus. Conversely, the basins of attraction of the discovered type I attractors in Fig. 12a intersect with

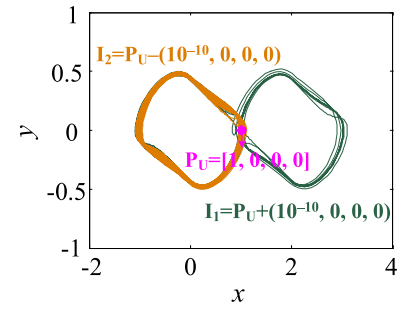

Fig. 14 Superimposed 2D $x - y$ plane views of type II attractors under initial conditions P_U and $I_{1,2}$

the system equilibria. However, the cross section of attracting basins in Fig. 12b is not enough to judge whether the discovered type II attractors are hidden attractors or self-excited attractors. Therefore, we use another method derived from the definition of hidden attractors for analysis. Selecting an unstable equilibrium point as the initial value of the system with parameter P_2, such as initial point $P_U = [1, 0, 0, 0]$, one can obtain a fixed point with magenta shown in Fig. 14. It is clear that the point attractor in Fig. 14 is a self-excited attractor. Inspired by [38], one can set up a small enough epsilon neighborhood $O_r(P_U)$, where r is the radius of a four-dimensional geometric structure centered at P_U. Obviously, when $r = 10^{-9}$, the points $I_{1,2} = P_U \pm (10^{-10}, 0, 0, 0)$ are all within $O_r(P_U)$. If $I_{1,2}$ are chosen as the initial values, the system will generate two type II attractors, as shown in Fig. 14. So this is sufficient to prove that the basins of attraction of the discovered type II attractors intersect with an equilibrium point, and in this sense, the type II attractors are not hidden. Therefore, the two types of bondorbital attractors in our paper are not hidden attractors.

In short, the bondorbital attractors in this paper are a new type of attractors, whose basic structures are generated differently from the traditional self-excited attractors (whose basic structures are generated around a single unstable equilibrium), and they are not in the category of hidden attractors.

4 Bondorbital attractors with discrete basins of attraction (type II attractors)

To demonstrate that the discrete basins of attraction in Fig. 12b are incomplete, we further simulate basins of attraction within a smaller range of initial condition

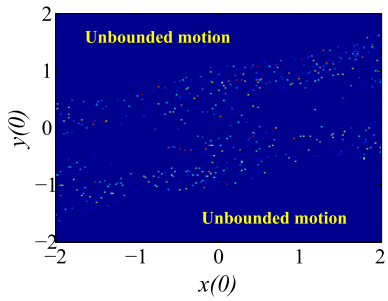

Fig. 15 Cross section at $z(0) = w(0) = 0$ in $x(0) - y(0)$ plane for system with parameter P_2, where $x(0), y(0) \in (-2, 2)$

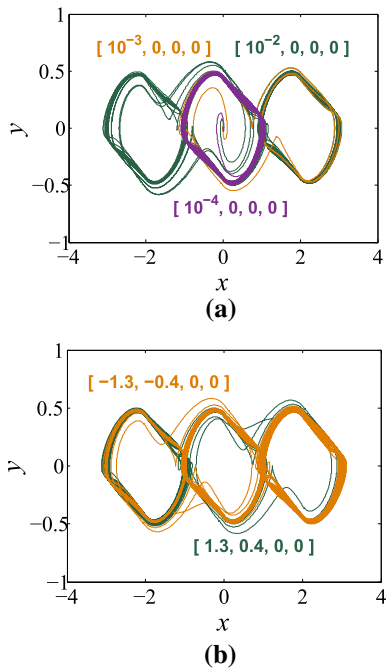

Fig. 16 Superposed 2D views of type II attractors in $x - y$ plane under some specific initial conditions

space, as shown in Fig. 15, in which the initial values $x(0)$ and $y(0)$ have an iteration point of 201, so the step size is 0.02. Due to smaller step size, much more discrete attracting basins of type II attractors are scattered in Fig. 15. This shows that because there are too many motion states simultaneously, it is impossible to carry out numerical simulation exactly, and the basins of attraction in Fig. 12b and even in Fig. 15 are incomplete. We present the phase portraits in $x - y$ plane under some specific initial conditions to explore more features, as shown in Fig. 16.

As per Fig. 15 and the coexistence of three type II attractors under the initial conditions of different orders of magnitude shown in Fig. 16a, it can be boldly inferred that the basin of attraction of each bondorbital attractor can be infinitely small and discretely distributed. It can also be explained from these that the system with parameter P_2 has infinitely many motion states in this case, that is, it has extreme multistability [53,54].

A comparative analysis of Figs. 2a, 3a, and 16a reveals that the type II attractors perform a kind of special motion, in which the central points and connection points of the ring structures are included in sets $\{0, \pm 2\}$ and $\{\pm 1, \pm 3\}$. However, these two sets correspond to the turning point values and the step values of the SFS $f(x, 1, 1)$ shown in Fig. 1, respectively. Table 2 shows that all the equilibria in these cases are the saddle-foci with index 1. These results are consistent with the theoretical analysis of the generation mechanisms for the bondorbital attractors in Sect. 2.4.

On account of the theoretical and experimental analyses, it can be inferred that the system with parameter P_2 based on SFS $f(x, 1, 1)$ can generate a bondorbital attractor having a threefold basic structures by finding a suitable initial condition. As expected, Fig. 16b shows the $x - y$ plane phase portraits of the type II attractors having triple-ring structure, the initial conditions of which are obtained by a loop test algorithm. Therefore, we are convinced that this kind of attractors is a new form that can be expanded based on every two adjacent homogeneous saddle-focus equilibria with index 1 but demand on initial conditions.

The bondorbital attractors shown in Figs. 17 and 18 can be obtained by choosing appropriate initial conditions if the SFS becomes $f(x, 2, 2)$. Figures 17 and 18 show the type II attractors with fourfold and fivefold structures, respectively, which prove our previous assumptions. These is a new type of extensible chaotic attractors that are different from the known multi-scroll, multi-wing, and multi-folded torus chaotic attractors [26]. Therefore, combining with the SFS $f(x, M, N)$ in this paper, the system with parameter P_2 can generate bondorbital attractors with at most $(N + M + 1)$-fold structures.

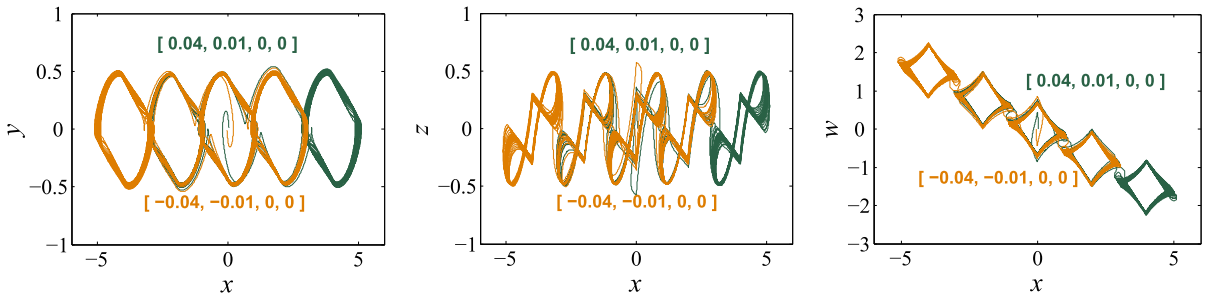

Fig. 17 Type II attractors with fourfold structures in **a** $x - y$, **b** $x - z$, and **c** $x - w$ plane

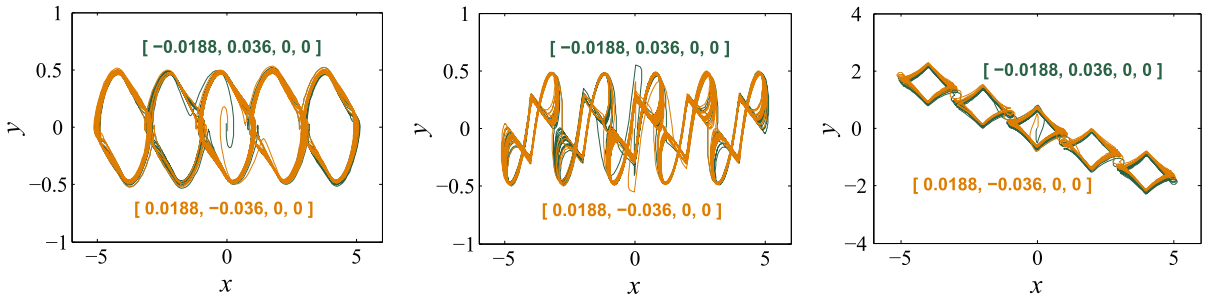

Fig. 18 Type II attractors with fivefold structures in **a** $x - y$, **b** $x - z$, and **c** $x - w$ plane

5 Summary of two classes of bondorbital attractors

In order to summarize the main characteristics of the two types of bondorbital attractors discovered in our chaotic system, a tabular form is adopted to compare the similarities and differences between them, as given in Table 3. From Table 3, we can see that the two kinds of bondorbital attractors have many interesting characteristics or complex dynamical behaviors, some of which are rarely found or possessed in available chaotic systems, such as large $|\sigma/\gamma|$, discrete basins of attraction, nonhyperchaotic but with Kaplan–Yorke dimension greater than 3. Maybe their strict requirements on initial conditions or system coefficients, these new types of attractors have not been reported.

6 Conclusions

Setting the system parameters $P_1 = (-1, 0.2, 1, 1.1, 0.001)$ and $P_2 = (-2.08, 0.2, 1, 1.1, 0.001)$, we find two kinds of unusual attractors in a 4D autonomous chaotic system with infinite equilibria, which are called bondorbital attractors in this article. In this paper, the numerical model of the system is given and its graph simulations as well as dynamics analysis are carried out based on a SFS $f(x, 1, 1)$. According to the eigenvalues at equilibrium points, the unstable equilibria of the system with parameters P_1 and P_2 are saddle-foci with index 1. The primary goal of this paper is to explore and analyze the generation mechanisms of the two kinds of unusual attractors as well as discover their unique features. Through comparative analysis, we prove that the basic structures of the discovered bondorbital attractors are different from the traditional self-excited attractors (whose basic structures are generated around a single unstable equilibrium), and they are not in the category of hidden attractors. The basic structures of the bondorbital attractors are bond orbits between two adjacent homogeneous saddle-focus equilibria with index 1. In this paper, the exploration and analysis of the bondorbital chaotic attractors in the proposed system may help to deepen the understanding of chaotic systems and enrich the types of chaotic attractors.

Table 3 The main characteristics of two categories of bondorbital attractors

Differences					Similarities			
System parameters	Basins of attraction	Hardware experiments	Special natures	Shilnikov inequalities $\lvert\sigma/\gamma\rvert < 1$ and $\lvert\sigma_i/\gamma_i\rvert < 1\ (i = 1, 2)$	D_{KY}	Symmetry	Equilibrium points	The absolute value of the ratio of σ to γ ($\lvert\sigma/\gamma\rvert$)
$P_1 = (-1,$ 0.2, 1, 1.1, 0.001)/type I attractors	Continuous basins of attraction (diagonal distribution)	Yes/ method of shorting a capacitor	Coexistence features	Mismatch ($\lvert -0.755/0.610\rvert > 1$)	> 3/ fractional dimensions (type I with 3.038 and type II with 3.158)	Symmetric regarding the origin	Saddle-foci with index 1	Large (type I with $\lvert -0.755/0.610\rvert \approx 1.238$ and type II with $\lvert -0.904/0.908\rvert \approx 0.996$)
$P_2 = (-2.08,$ 0.2, 1, 1.1, 0.001)/type II attractors	Discrete basins of attraction (incomplete form)	No/ hard or even cannot to achieve	Structural repeatability	Meet ($\lvert -0.904/0.908\rvert < 1$)				

Acknowledgements This research was supported by the National Natural Science Foundation of China (No. 61571185), the Science and Technology Planning Project of Hunan Province (2017GK4009), and the Open Fund Project of Key Laboratory in Hunan Universities (No. 18K010).

Compliance with ethical standards

Conflict of interest The authors declare that they have no conflict of interest.

References

1. Ruelle, D., Takens, F.: On the nature of turbulence. Commun. Math. Phys. **20**(3), 167–192 (1971)
2. Matsumoto, T., Chua, L.O., Komuro, M.: The double scroll. IEEE Trans. Circuits Syst. **32**(8), 797–818 (1985)
3. Suykens, J.A.K., Vandewalle, J.: Quasilinear approach to nonlinear systems and the design of n-double scroll (n = 1,2,3,4,). IEE Proc. G **138**(5), 595–603 (1991)
4. Sprott, J.C.: A new class of chaotic circuit. Phys. Lett. **266**(1), 19–23 (2000)
5. Yu, S.M., Lü, J.H., Leung, H., Chen, G.R.: Design and implementation of n-scroll chaotic attractors from a general Jerk circuit. IEEE Trans. Circuits Syst. I Regul. Pap. **52**(7), 1459–1476 (2005)
6. Elwakil, A.S.: Nonautonomous pulse-driven chaotic oscillator based on Chua's circuit. Microelectron. J. **33**(5–6), 479–486 (2002)
7. Hong, Q.H., Xie, Q.G., Xiao, P.: A novel approach for generating multi-direction multi-double-scroll attractors. Nonlinear Dyn. **87**(2), 1015–1030 (2017)
8. Zhang, X., Wang, C.H.: A novel multi-attractor period multi-scroll chaotic integrated circuit based on CMOS wide adjustable CCCII. IEEE Access **7**, 16336–16350 (2019)
9. Lorenz, E.N.: Deterministic non-periodic flow. J. Atmos. Sci. **51**(3), 130–141 (1963)
10. Chen, G.R., Ueta, T.: Yet another chaotic attractor. Int. J. Bifurc. Chaos **9**(7), 1465–1466 (1999)
11. Lü, J.H., Chen, G.R.: A new chaotic attractor coined. Int. J. Bifurc. Chaos **12**(3), 659–661 (2002)
12. Elwakil, A.S., Ozoguz, S., Kennedy, M.P.: Creation of a complex butterfly attractor using a novel Lorenz-type system. IEEE Trans. Circuits Syst. I Fundam. Theory Appl. **49**(4), 527–530 (2002)
13. Elwakil, A.S., Ozoguz, S., Kennedy, M.P.: A four-wing butterfly attractor from a fully autonomous system. Int. J. Bifurc. Chaos **13**(10), 3093–3098 (2003)
14. Yu, S.M., Lü, J.H., Tang, W.K.S., Chen, G.R.: A general multiscroll Lorenz system family and its realization via digital signal processors. Chaos **16**(3), 033126 (2006)
15. Yu, S.M., Tang, W.K.S., Lü, J.H., Chen, G.R.: Multi-wing butterfly attractors from the modified Lorenz systems. In: IEEE International Symposium on Circuits and Systems, pp. 768–771 (2008)

16. Yu, S.M., Tang, W.K.S.: Tetrapterous butterfly attractors in modified Lorenz systems. Chaos Solitons Fractals **41**(4), 1740–1749 (2009)
17. Yu, S.M., Tang, W.K.S., Lü, J.H., Chen, G.R.: Generation of n×m-wing Lorenz-like attractors from a modified Shimizu–Morioka model. IEEE Trans. Circuits Syst. II Express Briefs **55**(11), 1168–1172 (2008)
18. Yu, S.M., Lü, J.H., Chen, G.R., Yu, X.H.: Design and implementation of grid multiwing butterfly chaotic attractors from a piecewise Lorenz system. IEEE Trans. Circuits Syst. II Express Briefs **57**(10), 803–807 (2010)
19. Yu, S.M., Lü, J.H., Yu, X.H., Chen, G.R.: Design and implementation of grid multiwing hyperchaotic Lorenz system family via switching control and constructing super-heteroclinic loops. IEEE Trans. Circuits Syst. I Regul. Pap. **59**(5), 1015–1028 (2012)
20. Hong, Q.H., Xie, Q.G., Shen, Y., Wang, X.P.: Generating multi-double-scroll attractors via nonautonomous approach. Chaos **26**(8), 083110 (2016)
21. Matsumoto, T.: Chaos in electronic circuits. Proc. IEEE **75**(8), 1033–1057 (1987)
22. Yu, S.M., Lü, J.H., Chen, G.R.: Multifolded torus chaotic attractors: design and implementation. Chaos **17**(1), 013118 (2007)
23. Nishiuchi, Y., Ueta, T., Kawakami, H.: Stable torus and its bifurcation phenomena in a simple three-dimensional autonomous circuit. Chaos Solitons Fractals **27**(4), 941–951 (2006)
24. Yu, S.M., Lü, J.H., Chen, G.R.: Theoretical design and circuit implementation of multidirectional multi-torus chaotic attractors. IEEE Trans. Circuits Syst. I Regul. Pap. **54**(9), 2087–2098 (2007)
25. Tsvetelin, T.D., Gilmore, R.: Topological aspects of the structure of chaotic attractors in R-3. Phys. Rev. E **69**(5), 056206 (2004)
26. Lü, J.H., Chen, G.R.: Generating multiscroll chaotic attractors: theories, methods and applications. Int. J. Bifurc. Chaos **16**(04), 775–858 (2006)
27. Letellier, C., Gilmore, R., Jones, T.: Peeling bifurcations of toroidal chaotic attractors. Phys. Rev. E **76**(6), 066204 (2007)
28. Wang, Z.H., Sun, Y.X., Cang, S.J.: A 3-D spherical chaotic attractor. Acta Phys. Pol. B **42**(2), 235–247 (2011)
29. Letellier, C., Aguirre, L.A.: Required criteria for recognizing new types of chaos: application to the "cord" attractor. Phys. Rev. E **85**(3), 036204 (2012)
30. Wang, X., Chen, G.R.: Constructing a chaotic system with any number of equilibria. Nonlinear Dyn. **71**(3), 429C436 (2013)
31. Wang, Z.L., Cang, S.J., Wang, Z.H., Xue, W., Xue, W., Chen, Z.Q.: A strange double-deck butterfly chaotic attractor from a permanent magnet synchronous motor with smooth air gap: numerical analysis and experimental observation. Abstract and Applied Analysis **495126** (2014)
32. Qi, G.Y., van Wyk, B.J., van Wyk, M.A.: A four-wing attractor and its analysis. Chaos Solitons Fractals **40**(4), 2016–2030 (2009)
33. Guo, Y.L., Qi, G.Y., Hamam, Y.: A multi-wing spherical chaotic system using fractal process. Nonlinear Dyn. **85**(4), 2765–2775 (2016)
34. Cang, S.J., Wu, A.G., Wang, Z.L., Wang, Z.H., Chen, Z.Q.: A general method for exploring three-dimensional chaotic attractors with complicated topological structure based on the two-dimensional local vector field around equilibriums. Nonlinear Dyn. **83**(1–2), 1069–1078 (2016)
35. Chua, L.O., Komuro, M., Matsumoto, T.: The double scroll family. IEEE Trans. Circuits Syst. **33**(11), 1027–118 (1986)
36. Kuznetsov, N.V., Leonov, G.A., Vagaitsev, V.I.: Analytical-numerical method for attractor localization of generalized Chua's system. IFAC Proc. **43**(11), 29–33 (2010)
37. Leonov, G.A., Kuznetsov, N.V., Vagaitsevb, V.I.: Localization of hidden Chua's attractors. Phys. Lett. A **375**(23), 2230–2233 (2011)
38. Cang, S.J., Li, Y., Zhang, R.Y., Wang, Z.H.: Hidden and self-excited coexisting attractors in a Lorenz-like system with two equilibrium points. Nonlinear Dyn. **95**(1), 381–390 (2019)
39. Jafari, S., Sprott, J.C., Golpayegani, S.M.R.H.: Elementary quadratic chaotic flows with no equilibria. Phys. Lett. A **377**(9), 699–702 (2013)
40. Zhou, L., Wang, C.H., Zhou, L.L.: A novel no-equilibrium hyperchaotic multi-wing system via introducing emristor. Int. J. Circuit Theory Appl. **46**(1), 84–98 (2018)
41. Molaie, M., Jafari, S., Sprott, J.C., Golpayegani, S.M.R.H.: Simple chaotic flows with one stable equilibrium. Int. J. Bifurc. Chaos **23**(11), 1350188 (2013)
42. Jafari, S., Sprott, J.C.: Simple chaotic flows with a line equilibrium. Chaos Solitons Fractals **57**, 79–84 (2013)
43. Pham, V.T., Jafari, S., Volos, C., Kapitaniak, T.: A gallery of chaotic systems with an infinite number of equilibrium points. Chaos Solitons Fractals **93**, 58–63 (2016)
44. Witula, R., Slota, D.: Cardano's formula, square roots, Chebyshev polynomials and radicals. J. Math. Anal. Appl. **363**(2), 639–647 (2010)
45. Chang, T.S., Chen, C.T.: On the RouthCHurwitz criterion. IEEE Trans. Autom. Control **19**(3), 250–251 (1974)
46. Wolf, A., Swift, J.B., Swinney, H.L., Vastano, J.A.: Determining Lyapunov exponents from a time series. Physica D **16**(3), 285–317 (1985)
47. Kaplan, J., Yorke, J.: Functional Differential Equations and Approximation of Fixed Points. Lecture notes in mathematics, vol. 730, p. 228. Springer, Berlin (1979)
48. Silva, C.P.: Shil'nikov's theorem—a tutorial. IEEE Trans. Circuits Syst. I Fundam. Theory Appl. **40**(10), 675–682 (1993)
49. Smale, S.: Diffeomorphisms with many periodic points. In: Cairns, S.S. (ed.) Differential and Combinatorial Topology, pp. 63–80. Princeton University Press, Princeton (1965)
50. Wiggins, S.: Global Bifurcations and Chaos, Applied Mathematical Sciences. Springer, New York (1988)
51. Wang, C.H., Liu, X.M., Xia, H.: Multi-piecewise quadratic nonlinearity memristor and its 2N-scroll and 2N+1-scroll chaotic attractors system. Chaos **27**(3), 033114 (2017)

52. Nazarimehr, F., Rajagopal, K., Kengne, J., Jafari, S., Pham, V.T.: A new four-dimensional system containing chaotic or hyper-chaotic attractors with no equilibrium, a line of equilibria and unstable equilibria. Chaos Solitons Fractals **111**, 108–118 (2018)
53. Bao, B.C., Bao, H., Wang, N., Chen, M., Xu, Q.: Hidden extreme multistability in memristive hyperchaotic system. Chaos Solitons Fractals **94**, 102–111 (2017)
54. Zhou, L., Wang, C.H., Zhang, X., Yao, W.: Various attractors, coexisting attractors and antimonotonicity in a simple fourth-order memristive twin-T oscillator. Int. J. Bifurc. Chaos **28**(4), 1850050 (2018)